Transmission ion channeling analysis of isolated 60° misfit dislocations

M. B. H. Breese,[a] L. Huang, and E. J. Teo
Centre for Ion Beam Applications, 2 Science Drive 3, Department of Physics, National University of Singapore, Singapore 117542

P. J. C. King
Rutherford Appleton Laboratories, Chilton, OX11 OQX, United Kingdom

P. R. Wilshaw
Department of Materials, University of Oxford, Parks Road, Oxford, United Kingdom

(Received 11 July 2005; accepted 12 October 2005; published online 16 November 2005)

High-contrast transmission channeling images and linescans of isolated bunches and individual 60° misfit dislocations in thick partially relaxed $Si_{1-x}Ge_x$/Si layers are presented. Changes in dislocation contrast with tilt angle are explained using a model of planar dechanneling by the two-edge components of 60° dislocations. By careful analysis of the tilting contrast, all of the four possible combinations of the two-edge components of the Burger's vector of 60° dislocations may be distinguished. © *2005 American Institute of Physics*. [DOI: 10.1063/1.2135393]

Channeled ions have a smaller probability of scattering from lattice nuclei and a lower rate of energy loss compared to nonchannelled randomly oriented ions. This respectively produces a dip in the yield of backscattered ions and a peak in the energy of ions transmitted through thin crystals as a function of beam/crystal alignment.[1,2] The use of MeV proton beam currents of ~1 fA, focused to spot sizes of ~300 nm in a nuclear microprobe, was developed to produce spatially resolved transmission channeling images of defects in thinned crystals.[3] The samples are mechanically thinned and polished to a thickness of 20 μm, and a surface-barrier detector on the beam axis records the energy spectrum of the transmitted protons as the channeled beam scans over the surface. Planar channeled protons lose energy at typically one-half the rate of nonchanneled protons,[1,4] and any lattice disruption due to defects causes additional dechanneling and hence a local increase in energy loss. Transmission channeling images of variations in transmitted energy thus show the distribution of defects, such as misfit dislocations, in heavily relaxed silicon-germanium layers,[5,6] stacking faults,[7,8] precipitates,[9] and areas of elastic strain[10] and exfoliated regions.[11]

We have recently implemented a transmission channeling facility on a high-demagnification nuclear microprobe[12] which uses a quadrupole-lens triplet to focus MeV proton beams to spot sizes of ~50 nm.[13] Even with demagnifications of 220 and 60 in the horizontal and vertical directions, the focused beam convergence angle for transmission channeling measurements is only ~0.01°, much less than the planar channeling critical angle of 0.17° for 2 MeV protons in the silicon (110) planes. The counting statistics were also greatly improved[12] by only recording those transmitted protons which remained well channeled throughout the thinned crystal. This was achieved using a Mylar foil located in front of the detector which stopped the lower-energy dechanneled ions. The foil thus acted as an energy discriminator and greatly improved the statistics by discarding the large dechanneled beam fraction (typically 95%) which contributes no useful information.

This new facility has been used to record transmission channeling images and line scans of isolated bunches and individual misfit dislocations in a 1.8 μm thick $Si_{0.95}Ge_{0.05}$ epilayer grown on a [001] silicon substrate. The critical layer thickness for this layer thickness and composition is ~4 μm,[14] so the layer is mostly unrelaxed. However, some misfit dislocations are produced in localized regions at the $Si/Si_{0.95}Ge_{0.05}$ layer interface, probably nucleated on defects on the substrate surface. These 60° dislocations run along [110] and [1$\bar{1}$0] directions to form a cross pattern.[15,16] The crystal was given a Schimmel etch, which preferentially etches the highly strained cores of the threading segments on the surface,[17] resulting in a series of etch pits along each cross-arm. The Nomarski image in Fig. 1(a) shows a cross-arm running along the (110) and (1$\bar{1}$0) planes. By counting the number of etch pits (at higher magnification), the number of 60° dislocations in the boxed area of the cross-arm was determined to be five.

The transmission channeling images in Figs. 1(b)–1(d) were recorded from within the boxed area. Bright/dark areas

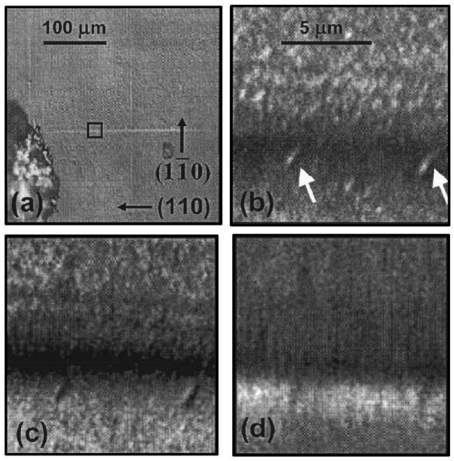

FIG. 1. (a) Low magnification Nomarski image. A marker of silver paint was placed at the left edge for the subsequent location of this cross. (b) to (d) Transmission channeling images of the 11×11 μm^2 boxed area shown in (a). The two arrowed oval features are etch pits. The beam tilt angles to the (110) planes are (b) +0.16°, (c) 0.00°, and (d) −0.16°.

[a]Electronic mail: phymbhb@nus.edu.sg

correspond to regions of high/low recorded counts, corresponding to good/poor channeling, respectively. The wide horizontally running band produced by the bunch of five dislocations lies along the (110) planes, with two etch pits visible. The two faint lines above this band, in Figs. 1(b) and 1(c), are interpreted as single dislocations; in Fig. 1(d), they are no longer resolved as the contrast merges with the main bunch. A change in contrast is observed at the bunch of five dislocations, from dark in Fig. 1(b) to dark/bright in Fig. 1(d). Figure 2(a) shows line scans recorded by scanning the focused beam in the vertical direction across this bunch of five dislocations, for different beam tilts to the substrate (110) planes. Figure 2(b) shows line scans recorded across the single dislocation located at the end of the same cross arm, where a similar, though weaker, contrast change is observed.

All components of the Burger's vector of 60° dislocations were considered to fully interpret these results. A 60° dislocation with a Burger's vector $b=(a/2)[101]$ and a line direction along $[1\bar{1}0]$ can be resolved into edge components $b_1=(a/4)[110]$, $b_2=(a/2)[001]$, and a screw component $b_3=(a/4)[1\bar{1}0]$, where a is the lattice parameter of silicon, equal to 0.543 nm. The edge component b_1 relieves the interfacial strain and its primary effect is to distort the (110) planes. If only the larger edge component b_2 is considered,

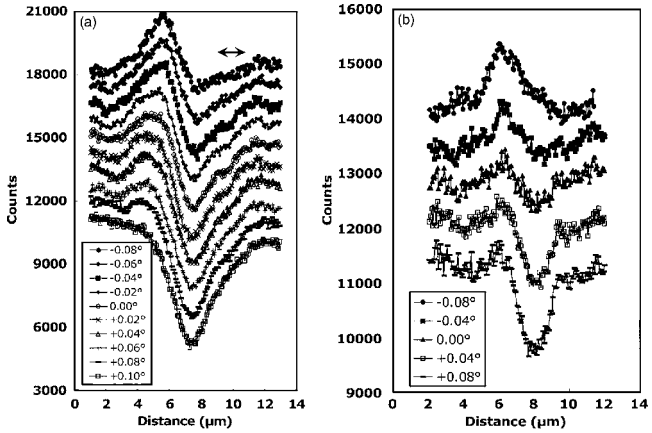

FIG. 2. (a) Vertical line scans recorded from the bunch of five dislocations for different tilt angles to the substrate (110) planes. Each spectrum is cumulatively offset by an additional 1000 counts on the vertical axis. The topmost line scan is for a tilt of −0.08° and the lowest for a tilt of +0.10°. (b) Similar line scans recorded across a single dislocation. The topmost line scan is for a tilt of −0.08° and the lowest for a tilt of +0.08°.

adjacent $[1\bar{1}0]$ dislocations in a bunch with the same sign of b_2 comprise a low-angle boundary, resulting in a local rotation of the (110) planes.[5,6,18]

Mazzer *et al.*[19] derived analytical formulae for the lattice plane distortion due to each of the screw and edge compo-

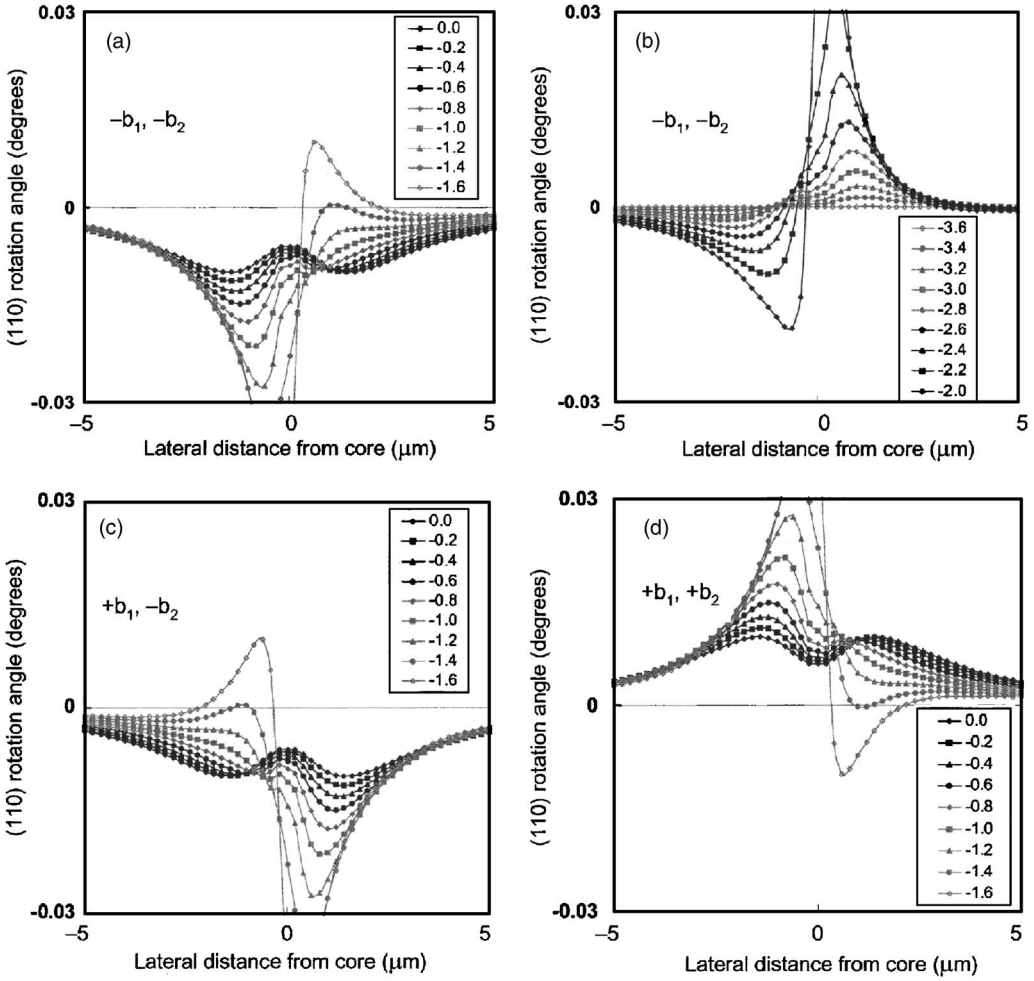

FIG. 3. Calculated (110) lattice plane rotation angle around a bunch of five 60° dislocations, at depth intervals of 0.2 μm beneath the surface. (a), (c), and (d) show the rotation from the surface (0.0 μm) to depths of −1.6 μm, and (b) from depths of −2.0 μm to −3.6 μm. The edge components are: (a) and (b) $-b_1$, $-b_2$, (c) $+b_1$, $-b_2$, and (d) $+b_1$, $+b_2$.

nents of 60° dislocations in their planar dechanneling backscattering study of heavily relaxed $In_xGa_{1-x}As/GaAs$. This planar channeling model used a harmonic approximation of the continuum potential in which perturbations are included as a lattice plane distortion function, which depends only on the geometry of the dislocation line and the channeling direction. We have calculated the lattice plane rotation as a function of lateral position away from the dislocation core and depth below the epilayer surface due to the two edge components using their formulae. The screw component may be ignored since it only distorts the orthogonal $(1\bar{1}0)$ planes, and has no effect on the horizontally running (110) planes.

Figure 3 shows the calculated (110) lattice plane rotation relative to the substrate (110) planes around a bunch of five 60° dislocations, for different depths beneath the epilayer surface. Protons will only be transmitted through the sample with high energy and recorded if they are channeled through the substrate, which will occur if they are channeled at the epilayer surface and remain channeled through the distorted epilayer. Figures 3(a) and 3(b) show the lattice plane rotation for b_1, b_2 both negative. When the beam is tilted positive with respect to the substrate (110) planes in Fig. 3(a), it is misaligned with the surface (110) planes which are all tilted in the negative sense. Hence, there is little probability that many protons will be channeled when the beam reaches the substrate, so a region of low counts will be recorded across the dislocation. When the beam is tilted negative with respect to the substrate (110) planes, it is tilted in the same sense as the epilayer surface, so many protons are initially channeled across the dislocation. However, the lattice planes become bent in the opposite senses on either sides of the dislocation core with increasing depth [Fig. 3(b)]. To the left-hand side of the dislocation core, the planes are always bent in the negative sense so there is a high probability that the protons will remain channeled, giving a region of high recorded counts. To the right-hand side of the dislocation core, the planes become bent in the positive sense with increasing depth. This greater overall bending and misalignment with the incident beam direction decreases the probability of the protons remaining channeled, producing a region of low recorded counts. The results in Figs. 1 and 2 are consistent with edge components b_1 and b_2, both negative along the length of this cross-arm.

For the combination $+b_1, -b_2$ [Fig. 3(c)], a dark band will still appear at positive tilts, but the locations of the bright/dark regions will be reversed at negative tilts. The sign of b_1 thus determines whether the dislocation appears bright/dark or dark/bright to one side of planar alignment. For the combination $+b_1, +b_2$ [Fig. 3(d)], the dislocation band will appear dark at a negative tilts. The sign of b_2 thus determines at which side of alignment the dislocation will appear dark. At positive tilts, the band will appear bright/dark on the left/right sides, respectively, whereas for the fourth combination, $-b_1, +b_2$ (not shown), the band will appear dark/bright. Hence, all four possible combinations of the two-edge components, $\pm b_1, \pm b_2$, can be distinguished by noting changes of dislocation contrast on tilting the sample.

Figure 3 demonstrates that any changes in the sign of either edge component along a cross-arm will cause the dislocation contrast to change. The Nomarski image in Fig. 4(a) shows a different cross on the same sample, with another fainter vertically running cross-arm visible to the left of the vertical cross-arm. Figure 4(b) shows a transmission channeling image of this area with the beam tilted just away from the $(1\bar{1}0)$ planes. The dark vertical band is produced by the main cross-arm. Along the length of the fainter cross-arm, the contrast changes from dark to bright. The two arrows mark the locations of the two etch pits corresponding to the region where the contrast changes. This suggests that these two extra dislocations cause the lattice planes to be tilted in the opposite sense, consistent with the sign of the Burger's vector component b_2 changing along this cross-arm.

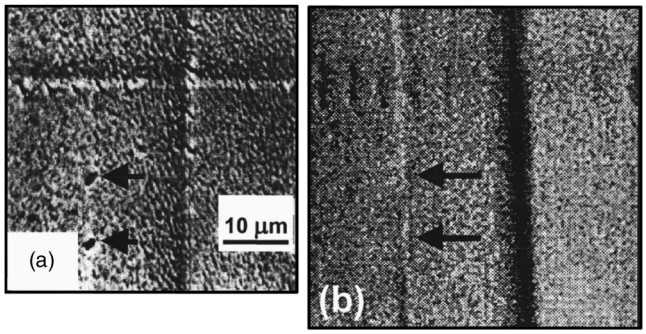

FIG. 4. (a) High magnification Nomarski image of a different cross-arm. The two arrowed oval features are etch pits. (b) Transmission channeling image of the same 40×40 μm^2 area. The locations of the two etch pits are arrowed.

This letter has shown that, by careful analysis of the tilting contrast with calculated results, any combination of edge components of the Burger's vector may be determined in transmission channeling analysis of 60° dislocations. An example where this has occurred has been identified.

[1] D. S. Gemmell, Rev. Mod. Phys. **46**, 129 (1974).
[2] L. C. Feldman, J. W. Mayer, and S. T. Picraux, *Materials Analysis by Ion Channeling* (Academic, New York, 1982).
[3] M. B. H. Breese, D. N. Jamieson, and P. J. C. King, *Materials Analysis Using a Nuclear Microprobe* (Wiley, New York, 1996).
[4] *Channeling, Theory, Observation and Applications*, edited by D. V. Morgan (Wiley, London, 1973).
[5] M. B. H. Breese, P. J. C. King, J. Whitehurst, G. R. Booker, G. W. Grime, F. Watt, L. T. Romano, and E. H. C. Parker, J. Appl. Phys. **73**, 2640 (1993).
[6] M. B. H. Breese, P. J. C. King, P. J. M. Smulders, and G. W. Grime, Phys. Rev. B **51**, 2742 (1995).
[7] P. J. C. King, M. B. H. Breese, P. R. Wilshaw, and G. W. Grime, Phys. Rev. B **51**, 2732 (1995).
[8] P. J. C. King, M. B. H. Breese, P. J. M. Smulders, P. R. Wilshaw, and G. W. Grime, Phys. Rev. Lett. **74**, 411 (1995).
[9] P. J. C. King, M. B. H. Breese, D. Meekeson, P. J. M. Smulders, P. R. Wilshaw, and G. W. Grime, J. Appl. Phys. **80**, 2671 (1996).
[10] P. J. C. King, M. B. H. Breese, P. J. M. Smulders, A. J. Wilkinson, G. R. Booker, E. H. C. Parker, and G. W. Grime, Appl. Phys. Lett. **67**, 3566 (1995).
[11] M. B. H. Breese, L. C. Alves, T. Hoechbauer, and M. Nastasi, Appl. Phys. Lett. **77**, 268 (2000).
[12] M. B. H. Breese, E. J. Teo, M. A. Rana, L. Huang, J. A. van Kan, F. Watt, and P. J. C. King, Phys. Rev. Lett. **92**, 045503 (2004).
[13] J. A. van Kan, A. A. Bettiol, and F. Watt, Appl. Phys. Lett. **83**, 1629 (2003).
[14] R. People and J. C. Bean, Appl. Phys. Lett. **47**, 322 (1985).
[15] C. G. Tuppen, C. J. Gibbings, and M. Hockly, J. Cryst. Growth **94**, 392 (1989).
[16] C. J. Gibbings, C. G. Tuppen, and M. Hockly, Appl. Phys. Lett. **54**, 148 (1989).
[17] D. G. Schimmel, J. Electrochem. Soc. **126**, 479 (1979).
[18] D. Hull, *Introduction to Dislocations* (Pergamon, Oxford, 1975).
[19] M. Mazzer, A. V. Drigo, F. Romanto, G. Salviati, and L. Lazzarini, Phys. Rev. B **56** 6895 (1997).